Title:

Leaf form diversification in an heirloom tomato results from alterations in two different *HOMEOBOX* genes

Short Title: Genetic basis of leaf shape variation between tomato cultivars

Hokuto Nakayama[a,†], Steven D. Rowland[a], Zizhang Cheng[a], Kristina Zumstein[a], Julie Kang[b], Yohei Kondo[c] and Neelima R. Sinha[a,*]

[a]Department of Plant Biology, University of California Davis, One Shields Avenue, Davis, CA 95616, U.S.A.

[b]Biology Department, 144 McCollum Science Hall, University of Northern Iowa, Cedar Falls, IA 50614, U.S.A.

[c]Division of Quantitative Biology, Okazaki Institute for Integrative Bioscience, National Institute for Basic Biology, National Institutes of Natural Sciences, Myodaiji, Higashiyama 5-1, Okazaki, Aichi 444-8787, Japan

[†]Current address: Graduate School of Science, Department of Biological Sciences, The University of Tokyo, Science Build. #2, 7-3-1 Hongo Bunkyo-ku Tokyo, 113-0033, Japan

[*]To whom correspondence should be addressed. Email: nrsinha@ucdavis.edu

Contact Information

Hokuto Nakayama: hokuto@bs.s.u-tokyo.ac.jp

Steven D. Rowland: sdrowland@ucdavis.edu

Zizhang Cheng: chengxiaoyi_01@sina.com

Kristina Zumstein: kmsarte@ucdavis.edu

Julie Kang: julie.kang@uni.edu

Yohei Kondo: y-kondo@nibb.ac.jp

Neelima R. Sinha: nrsinha@ucdavis.edu

Keywords: *BEL-LIKE HOMEODOMAIN*, *BIPINNATA*, evolution, leaf, *SOLANIFOLIA*, *Solanum lycopersicum*, Tomato, *WUSCHEL RELATED HOMEOBOX 1*

Abstract

Domesticated plants and animals display tremendous diversity in various phenotypic traits and often this diversity is seen within the same species. Tomato (*Solanum lycopersicum*; Solanaceae) cultivars show wide variation in leaf morphology, but the influence of breeding efforts in sculpting this diversity is not known. Here, we demonstrate that a single nucleotide deletion in the homeobox motif of *BIPINNATA*, which is a *BEL-LIKE HOMEODOMAIN* gene, led to a highly complex leaf phenotype in an heirloom tomato, Silvery Fir Tree (SiFT). Additionally, a comparative gene network analysis revealed that reduced expression of the ortholog of *WUSCHEL RELATED HOMEOBOX 1* is also important for the narrow leaflet phenotype seen in SiFT. Phylogenetic and comparative genome analysis using whole-genome sequencing data suggests that the *bip* mutation in SiFT is likely a *de novo* mutation, instead of standing genetic variation. These results provide new insights into natural variation in phenotypic traits introduced into crops during improvement processes after domestication.

Main

Domestication and subsequent improvement processes have made animals and plants more suitable for agriculture and achieved improvement in their usability, quality, and yield (1). In contrast to domestication, usually occurring once for many crops, selection for improvement happened multiple times and in numerous locations, leading to varieties adapted to local conditions and needs (2). Consequently, many crops show fascinating morphological diversity. Indeed, Darwin focused on this morphological diversity more than 150 years ago and postulated that knowledge of the mechanisms underlying diversity generated under human selection would provide general principles for understanding the process of evolution under natural selection (3). Domesticated tomato, *Solanum lycopersicum* L. (Solanaceae), is one of the most economically important vegetable crops in the world (4). The domesticated tomato exhibits tremendous morphological variation because of a long breeding history (5). Additionally, many heirloom tomatoes, varieties passed down through several generations within a family or specific regions, have an interesting breeding history predating 1940 when commercial hybrids first started becoming available. These

heirloom cultivars, when compared to commercial tomatoes, show morphological variation and flavor profiles that are often favored by gardeners (6). Many heirloom tomatoes contain genetic loci that affect most of the target flavor chemicals to improve the flavor of modern commercial tomato (7), making heirloom tomatoes an interesting resource for research on tomato improvement. Silvery Fir Tree (SiFT) is a traditional Russian heirloom tomato (6). SiFT has a highly complex leaf phenotype, with leaflets that are narrower than those seen in processing tomatoes such as M82 (Figure 1A to 1D). Interestingly, SiFT is sometimes used as an ornamental and landscaping plant rather than a crop due to the unique leaf shape in this variety, although SiFT does produce edible fruit (6). However, the genetic basis underlying the unique leaf morphology and breeding history of this cultivar is still unknown.

Here, we used a cross between SiFT and M82 to generate a mapping population and identified a single nucleotide deletion in the homeobox motif of a *BEL-LIKE HOMEODOMAIN* (*BELL*) gene, leading to a premature stop codon, and the highly complex leaf phenotype in SiFT. Based on genome sequencing, the *bip* mutation in SiFT is a *de novo* mutation that was not introgressed from other cultivars or wild

83 species. Further, we use a combination of gene co-expression network analysis and
84 CRISPR-Cas9 knockout mutants to show that reduced expression of the *WUSCHEL*
85 *RELATED HOMEOBOX 1* (*WOX1*) ortholog is also important for the narrower leaflet
86 phenotype and reduced leaf vascular density in SiFT. Additionally, we show that the
87 classic tomato leaf mutation, *solanifolia,* is caused by mutations in the same *WOX1*
88 gene. These results provide insights into natural variation in phenotypic traits
89 introduced into heirloom tomatoes during improvement after domestication.
90

Results

SiFT has increased leaf complexity and reduced vascular density compared to M82

Leaf complexity (LC) in SiFT is higher than that in M82 (Fig. 1A to 1C). The observation of gross leaf morphology showed distinct morphological differences between M82 and SiFT starting from the 1st formed leaves (Fig. 1D). While leaf primordia from Plastochron1 (P1) to P3 stages are not strikingly different between the cultivars, from P4 stage onward, difference in the number of leaflet primordia are consistently observed between M82 and SiFT (Fig. 1E). Thus, SiFT leaf primordia at P4 and older stages are more active in generating leaflets compared to M82 leaves at the same developmental stage, and have a prolonged morphogenetic window compared to that in M82. Previous studies have shown leaf vascular density (LVD) variation among cultivars and mutants (8). Although no difference was observed in leaf anatomy around the midvein (Supplementary Fig. 1), LVD was different between M82 and SiFT (Fig. 1F). Therefore, SiFT differs from M82 in leaf complexity, developmental trajectory, and vascular density.

SiFT has a mutation in a *BEL-LIKE HOMEODOMAIN* gene, *BIPINNATA*

To identify genes involved in the regulation of leaf complexity (LC), bulked segregant analysis (BSA) on an F2 population (198 individuals) derived from a cross between M82 and SiFT was utilized (Supplementary Fig. 2). Two phenotypically defined bulks showing difference in LC (High-LC bulk and Low-LC bulk; Supplementary Fig. 3) were used to detect a locus between 45000000 and 55000000 bp on chromosome 2 that controlled LC (Fig. 2A; top and Supplementary Fig. 4). Whole genome sequencing of SiFT was used to define sequence variants in the genome including the region defined by BSA. However, we detected more than 100 variants in this region in the SiFT genome (Fig. 2A; middle). To narrow down the number of candidates, we used Protein Variation Effect Analyzer (PROVEAN), which allows us to predict whether an amino acid substitution or indel has an impact on the biological function of a protein (Supplementary Fig. 2) (9). The PROVEAN analysis found only one deleterious variant in the region (Fig. 2A; bottom), located in the *BIPNNATA* (*BIP*: Solyc02g089940) gene (Fig. 2B), which is known to encode a BEL-LIKE HOMEODOMAIN (BLH) protein (10). *BIP* is located in the *BLH* clade in the *BELL/KNOX1* phylogeny (Supplementary

Fig. 5). The 1 bp deletion at position 1674 within the homeobox domain generates a premature stop codon, and as a result the BIP protein is truncated in SiFT (Fig. 2B and 2C, and Supplementary Fig. 6). Additionally, we confirmed that the genome of a different SiFT accession, previously sequenced by Tieman and coworkers, also has the same *bip* mutation (7) (Supplementary Fig. 7).

Highly complex leaf phenotype seen in SiFT is caused by the *bip* mutation

To verify the effect of the *bip* mutation on leaf phenotypes we investigated the morphology and early development of leaves in *bip3*, a *bip* mutant in the M82 background (12). LC in *bip3* was similar to that of SiFT (Fig. 3A and 3B). Additionally, we confirmed that *bip3* leaf primordia are active in generating multiple leaflets at the P4 stage as seen in SiFT (Fig. 3C). Although the *BIP* gene has been studied in Arabidopsis and tomato, the expression pattern of the *bip* gene in leaf primordia is not known (10, 11). We performed whole-mount *in situ* hybridization and detected *BIP* gene expression in the proximal part of leaf primordium, where leaflet primordia emerge (Fig. 3D). A previous study showed that the expression of *TOAMTO KNOTTED-1* (*Tkn1*), the

ortholog of Arabidopsis *KNOX1* gene *BREVIPEDICELLUS*, is increased in the *bip* mutant (10). Quantitative RT-PCR (qPCR) was used to detect elevated level of *Tkn1* expression in SiFT compared to M82 (Fig. 3E). It is known that *KNOX* overexpression increases leaf complexity (12). These data suggest that the highly complex leaf phenotype seen in SiFT is caused by high expression of *Tkn1* facilitated by the *bip* mutation.

Although LC in *bip3* is quite similar to SiFT, the two genotypes have distinctly different leaflet shapes. Deep learning-based nonlinear PCA with leaflet shapes in M82, *bip3*, and SiFT suggested that *bip3* leaf shape is different from that of M82 but not the same as SiFT (Fig. 3F). This trend was confirmed by different methods (Supplementary Fig. 8). Indeed, leaflets of SiFT are narrower than those of bip3 (Fig. 3G). Additionally, LVD in *bip3* is similar to that of M82 and differs from that of SiFT (Fig. 3H and 3I). Thus, the mutation at the *BIP* locus is not sufficient to explain all the leaf phenotypes seen in SiFT.

Gene co-expression network analysis suggests a role for Sl *WOX1* in regulating leaf phenotypes

To investigate the molecular basis for leaf phenotypes seen in SiFT, we performed RNA-seq and compared differentially expressed genes (DEGs) between M82 and SiFT (Supplementary Table 1). However, the large number of DEGs precluded identification of genes critical in generating differences in leaf shape between two genotypes. Gene co-expression network (GCN) analysis can reveal biologically relevant information to identify molecular mechanisms underlying biological processes (13). Therefore, we constructed GCNs with RNA-seq data of M82 and SiFT and compared these networks to identify key genes responsible for the leaf phenotypes seen in SiFT. The genes used for the network analysis included a set of literature-curated genes involved in leaf development (14). The GCN for M82 showed differences in network structure, edge number, node number, and average of degree between genes when compared to the GCN for SiFT (Fig. 4A and Supplementary Table 2), indicating that many genes involved in leaf development are differentially expressed between the two genotypes. Community structure in the networks was analyzed based on the fast greedy modularity

optimization algorithm and GO enrichment analysis by community was performed (14). Two communities (community 1: C1 and community 2: C2) predominate in both networks (Fig. 4A), and GO enrichment analysis by community showed that community 1 is enriched for the same GO terms between M82 and SiFT networks, in particular, GO terms with higher Fold enrichment (>50; full result of the GO enrichment analysis, Supplementary Table 3). On the other hand, community 2 is different between the two networks (Fig. 4B and Supplementary Table 3). In community 2 of the M82 GCN, GO terms such as “cytokinin biosynthetic processes” (GO: 0009691), “cytokinin metabolic process” (GO:0009690), “regulation of cell cycle arrest” (GO: 0071156), and “cellular hormone metabolic process” (GO:0034754; Supplementary Table 3) were more than 100 fold enriched. However, there were no enriched GO terms with high fold enrichment in community 2 of the SiFT GCN (Fig. 4B and Supplementary Table 3), suggesting that genes in community 2 might be crucial for explaining differences in leaf phenotype between M82 and SiFT. To compare the two networks and identify the differences between them, we performed comparative network analysis using the R package "DiffCorr" (15). DiffCorr allows us to find

186 statistically significant differences between two networks. The DiffCorr analysis
187 identified 160 DiffCorr genes, which are differentially correlated genes between two
188 networks (Supplementary Table 4). Those genes should have distinct expression pattern
189 between M82 and SiFT. The 160 DiffCorr genes have distinct expression profiles
190 between M82 and SiFT (Fig. 4C). Additionally, many genes having more differential
191 correlations between two networks show distinct expression patterns, suggesting that
192 those DiffCorr genes are responsible for the difference between the two networks (Fig.
193 4C). The DiffCorr analysis revealed a *WOX*-like gene (Solyc03g118770) as the most
194 significantly different between the M82 and SiFT GCNs (Supplementary Table 4) and
195 the gene was located in community 2 of the M82 GCN (Supplementary Table 5). Based
196 on phylogenetic analyses and alignments, the *WOX*-like gene is the tomato ortholog of
197 Arabidopsis *WOX1* (Sl *WOX1*; Supplementary Fig. 9 and Supplementary Fig. 10). To
198 understand the role of Sl *WOX1* in leaf development, we focused on the Sl *WOX1* sub-
199 network which consisted of genes showing a direct connection to the Sl *WOX1*. This
200 sub-network showed that the Sl *WOX1* gene is connected to many genes involved in
201 leaf development in M82 GCN (Fig. 4D). Sl *WOX1* expression in SiFT leaf primordia

was lower than in M82 samples (Fig. 4E). To check the expression pattern of Sl *WOX1*, we performed whole mount *in situ* hybridization. Sl *WOX1* was expressed at the margins of leaf primordia and leaflet primordia (Figures 4F and 4G). This expression pattern was unaltered in SiFT (Supplementary Fig. 11). *WOX1* is known to express in leaf primordia and is involved in leaf lamina expansion in various plant species (16, 17). Moreover, in the *Medicago truncatula wox1* mutant, leaf vein density was lower than in wildtype (17). Therefore, Sl *WOX1* is likely a candidate gene for controlling both leaf width and leaf vein density in tomato.

Sl *WOX1* is involved in leaf lamina expansion and leaf vascular development

Sl *WOX1* is located on the long arm of chromosome 3 (Solyc03g118770; https://solgenomics.net/feature/17777644/details) and previous studies in several plant species indicate that the *wox1* mutants have narrower leaflets and low LVD (16, 17). Therefore, we mutated Sl *WOX1* in M82 plants using the CRISPR/Cas9 system and obtained a null mutation, referred to here as CR-*wox1-1* (Fig. 5A). CR-*wox1-1* plants showed narrower leaves (Fig. 5B and 5C) and lower LVD than M82 (Fig. 5D),

218 matching the phenotype described in *wox1* mutants in other species (16, 17). We
219 noticed that these phenotypes are quite similar to those of a classical tomato mutant,
220 *solanifolia* (*sf*). *sf* is known to have narrower leaflets and reduced vascular density (18)
221 and our rough mapping of the *solanifolia* mutation had identified a genomic location
222 close to that known for the *WOX1* locus (at the end of chromosome 3; Supplementary
223 Fig. 12). We obtained the two known alleles of the mutation (*sf* and *sf^wl*) and another
224 allele (e1862) from the Tomato Genetics Resource Center (TGRC;
225 http://tgrc.ucdavis.edu) and Genes that makes Tomato
226 (http://zamir.sgn.cornell.edu/mutants/), respectively. *sf*, *sf^wl*, and e1862 arose in the
227 Pearson, ROMA, and M82 backgrounds, respectively. *sf* has a 1 bp substitution (G to
228 A) at position 230 in Sl *WOX1* resulting in an amino acid swap from arginine to
229 histidine in the conserved homeodomain (Fig. 5A and Supplementary Fig. 13). *sf^wl*
230 and e1862 have a 1 bp substitution (G to A) at a splice site between intron 3 and exon 4,
231 which results in 10 bp shift to the next splice site (Supplementary Fig. 13 and
232 Supplementary Fig. 14). As a result, these mutants have a 10 bp deletion from position
233 595 to 604 resulting in a premature stop codon, which truncates the WOX1 protein such

234 that it lacks the conserved WOX domain (Fig. 5A and Supplementary Fig. 13 and
235 Supplementary Fig. 14). All these mutants showed narrower leaflets and low LVD
236 compared to their background genotypes (Fig. 5B to 5D). Hence, phenotypes seen in
237 these classical mutants were same as that of CR-*wox1-1*. Hereafter, we refer to the Sl
238 *WOX1* gene as *SOLANIFOLIA* (*SF*). These results indicated that *SF* functions in leaflet
239 outgrowth and vascular development in tomato leaves, performing a role similar to that
240 of *WOX1* in Arabidopsis and Medicago (16, 17, 19). These results confirm the role of
241 reduced expression of *SF* in conferring narrower leaflet and lower LVD phenotypes in
242 SiFT. Promoter sequences of *SF* in SiFT show no SNPs compared to the reference
243 tomato genome (Supplementary Fig. 15), coincident with the fact that the pattern of
244 expression *SF* is unaltered in SiFT compared to M82 (Supplementary Fig. 11). A
245 previous study suggested that *ARF3* suppresses *WOX1* expression in Arabidopsis (20).
246 In SiFT, expression level of the *ARF3* ortholog (Solyc02g077560) was higher than that
247 seen in M82 (Supplementary Fig. 16A) and the *ARF3* ortholog is known to be
248 expressed in leaf primordia (21). Additionally, the SiFT *ARF3* promoter has a SNP that
249 generated a new ZF-HD motif, which is known to be involved in binding of HB33

transcription factor (22) (Supplementary Fig. 16B). This *HB33* ortholog in Toamto (Solyc04g080490) is expressed in leaf primordia (Supplementary Fig. 17). Therefore, this gain-of-function SNP might explain the alteration in *SF* repression in SiFT.

bip sf double mutant shows highly complex, narrow leaves, and low LVD

Since SiFT has a *bip* mutation and *SF* repression, we generated a *bip sf* double mutant to investigate leaf phenotypes. Leaves in double mutant between *bip3* and e1862 had more leaflets than those of e1862 and the leaflets were narrower than those of *bip3* (Fig. 6A). Sometimes, secondary leaflets were observed on the 4th leaf (Fig. 6B) and the secondary leaflets became more obvious in higher order leaves in the double mutant (Fig. 6C). Additionally, LVD in the double mutant was lower than that in *bip3* (Fig. 6D), suggesting that these phenotypes are additive. Moreover, these trends were confirmed by another double mutant with a different combination of mutants (Supplemental Fig. 18). However, leaf morphology in the double mutant was not exactly the same as that of SiFT. Leaflets in leaves of SiFT have many robes (Fig 1B), leaves of the double mutant, however, do not have obvious lobes (Fig. 6A and

Supplemental Fig. 18). This may be due to the difference between reduced expression and complete loss of function of the *SF* in the two genotypes. Indeed, *sf* single mutants having truncated WOX1 protein such as CR-*wox1-1, sf^wl*, and e1862 do not have any lobes on leaves, whereas a weaker phenotype mutant, *sf*, shows lobed leaves (Fig. 5B). These results suggest that a mutation at *bip* and *WOX1* repression lead to highly complex and narrower leaves with reduced leaf vein density in SiFT, respectively (Fig. 6E).

Phylogenetic placement of SiFT and the *bip* mutation

Several mutations at the *BIP* locus have been described (10). However, the *BIP* mutation in the SiFT genome is different from these. Although previous studies constructed phylogenies with heirloom tomatoes (23), they were generated with whole-genome sequencing data. In order to understand the history of the *bip* mutation on chromosome 2, we first constructed a phylogenetic tree based on whole-genome sequencing data from 106 heirloom tomatoes (http://www.tomatogenome.net/accessions.html) to know the rough relationship

among them (Supplemental Fig. 19). Subsequently, we constructed a phylogenetic network using the "PhyloNetworks" package in Julia (24) to estimate whether introgressions from other tomatoes occurred in SiFT or not. This package allows us to discern various biological processes such as hybridization, introgression, or horizontal gene transfer. We used sequences around the *BIP* locus on chromosome 2 from 32 representative tomatoes based on the phylogeny with 106 heirloom tomatoes. *S. pimpinellifolium*, which is thought to be the progenitor wild species for domesticated tomato, was used as an outgroup in the heirloom tomato phylogeny. *S. cheesemaniae* and *S. lycopersicum* var. *cerasiforme* were also used (Fig. 7A). The network indicated that a US heirloom tomato, Giant Oxheart (GiO), is sister to SiFT, however GiO does not show the highly complex leaf phenotype characteristic of SiFT and lacks the mutation in *BIP* (Fig. 7B and 7C). The phylogeny suggests that Druzba is the result of a cross between an ancestor of Glacier and an ancestor of Giant Oxheart/SFT. However, the *bip* mutation seen in SiFT does not exist in Druzba either (Fig. 7B and 7C). Additionally, the wild species, *S. pimpinellifolium* (Fig. 7D), and the other tomato varieties do not harbor the SiFT specific mutation at *BIP* (Supplemental Fig. 19 and

298 Supplementary Table 6). These data suggest that the *bip* mutation in SiFT is likely a *de*

299 *novo* mutation, instead of standing genetic variation.

300

Discussion

We found that SiFT, an heirloom tomato, has a highly complex leaf phenotype and carries a mutation in the *BIP* gene, which encodes a *BEL-LIKE HOMEODOMAIN* protein (Solyc02g089940). Leaf complexity in the *bip3* mutant was remarkably similar to that of SiFT. *BIP* is expressed at the proximal end of developing leaf primordia, where leaflet primordia emerge. Previous studies demonstrated that *KNOXI* genes are overexpressed in leaves of *bip* mutants (10, 11) and the overexpression of *KNOX1* gene in leaves dramatically increases leaf complexity by prolonging specific stages of leaf development (25). Indeed, *Tkn1*, a tomato *KNOX1* gene, is highly expressed in SiFT leaf primordia and SiFT and *bip3* leaf primordia exhibit prolonged morphogenesis. In Arabidopsis, *saw1 saw2* double mutant showing ectopic *KNOX1* expression has increased leaf serrations (10, 11), indicating that *BLH* genes including *BIP*, *SAW1*, and *SAW2* act to limit leaf margin growth and the function appears to be conserved between them. Therefore, the *bip* mutation found in SiFT is the likely cause of increasing in *Tkn1* expression, prolonging morphogenesis, and increasing complexity in SiFT leaf primordia. We also found that leaflet shape in SiFT is narrower than *bip3*, which is

317 confirmed by deep learning-based nonlinear PCA and leaf shape analysis. Additionally,
318 leaf vein density in SiFT was lower than in *bip3*. To identify the genetic alterations
319 beyond *BIP* that explain the rest of leaf phenotypes seen in SiFT, we used comparative
320 gene co-expression network analysis. The *WOX1* ortholog (Solyc03g118770) had the
321 most altered correlations between the M82 and SiFT co-expression networks. The
322 expression level of the *WOX1* ortholog in SiFT is lower than M82. Additionally, *wox1*
323 mutants in Arabidopsis and Medicago are known to have narrower leaves compared to
324 WT (16, 17). A CRISPR/Cas9 *wox1* mutant in Tomato showed narrower leaves and
325 lower vascular density compared to WT. Moreover, we found that a classical tomato
326 mutant, *solanifolia (sf)*, harbored a deleterious mutation in the *WOX1* ortholog and
327 those *sf* mutants showed narrower leaves and lower vascular density. Whole-mount in
328 situ hybridization demonstrated that, similar to Arabidopsis and Medicago (16, 17), *SF*
329 is also expressed at the margin of tomato leaf and leaflet primordia, consistent with the
330 phenotype of leaf margins in *sf* mutants. In Arabidopsis, *WOX* genes promote lamina
331 outgrowth through regulation of cell proliferation in cells expressing *WOX1* and their
332 surrounding cells (16). Since leaf vascular development is influenced by this marginal

333 blade outgrowth (26), we propose that *SF* functions in leaf lamina outgrowth and
334 couples this growth feature with vascular patterning. The causal mutation that leads to
335 *SF* repression in SiFT might be a SNP in ARF3 promoter region in the SiFT genome,
336 however this needs further analysis. *WOX1* is present in the early-diverging angiosperm,
337 *Amborella trichopoda* (27), but the ancestral function in angiosperms is still unknown.
338 Additionally, no *WOX1* homologs have been identified in monocots (17, 28). These
339 facts suggest that the function of this *WOX1* gene in leaf development appears to be
340 conserved at least across the eudicots (e.g. Arabidopsis, Medicago, and Tomato).
341 Leaves of *bip* and *sf* double mutants are more complex than those of *wox1* and narrower
342 than those of *bip3*. Moreover, the double mutant showed low LVD. A recent study
343 suggested that the regulation of local growth and differentiation in leaf primordia leads
344 to diversity in leaf shape (29). *BIP* and *SF* are thought to regulate local growth and
345 differentiation in leaf primordia: *BIP* functions in the proximal part of leaf primordia
346 and *SF* functions at the marginal part. Therefore we conclude that the highly complex
347 and narrower leaf with reduced leaf vein density seen in SiFT is caused by a

348 combination of a mutation at *bip* and another as yet unknown second site mutation that
349 leads to *SF* repression (Fig. 8).
350 A phylogenetic tree constructed with WGS data and a phylogenetic network constructed
351 with sequences around *BIP* locus revealed that German Red Strawberry and Giant
352 Oxheart are sister to SiFT, respectively. However, they lack the *BIP* mutation and have
353 regular leaf shape. Moreover, none of the other varieties or wild species harbor the same
354 mutation at *BIP* seen in SiFT. Although a wild tomato species *S. galapagense* has
355 increased leaf complexity, the increased leaf phenotype is linked to promoter alterations
356 in an atypical *KNOX1* gene *PETROSELENUM*, not in *BIP* (10). Therefore, these data
357 indicate that the *BIP* mutation seen in SiFT is a *de novo* mutation that occurred during
358 breeding and is not likely to be an introgression from other varieties or wild species.
359 These are consistent with the fact that there is no cultivated tomato showing SiFT-like
360 leaf shape. This uniqueness of leaf shape in SiFT is achieved by the combination of a
361 mutation at *bip* and *SF* repression, leading to use of this variety as an ornamental and
362 landscaping plant (6). Emerging data suggest that leaflet shape affects fruit sugar
363 content in tomato (30, 31). Therefore, identification of these novel mutations not only

364 provides new insights into the breeding history of heirloom tomatoes, but also suggests

365 potential targets for enhancing sugar content to improve fruit quality in tomato.

366

Methods

Plant Materials

The following lines and mutants were provided by the Tomato Genetics Resource Center, University of California, Davis (USA; https://tgrc.ucdavis.edu/): *S. lycopersicum* cv M82 (LA3475), *sf*^wl (LA2012), *sf* (LA2311), and Pearson (LA0012). SiFT and ROMA were from our own stocks. *bip3* (e1444m2) was obtained from the saturated mutation library of tomato (32). e1862 was obtained from the Genes that makes Tomato (Israel; http://zamir.sgn.cornell.edu/mutants/).

Growth conditions

Tomato seeds were soaked in 50% bleach for 10 min, rinsed 3 times with water, and placed on water dampened paper towel in Phytatrays (Sigma Aldrich). Seeds were incubated in the dark at room temperature for 3 days then transferred to a growth chamber set at 22°C under long-day conditions (16 h light; 8 h dark) for 4 days. After approximately 7 days, seedlings had expanded cotyledons. These were then transplanted to 24-cell seedling propagation trays and grown in the chamber for a 35 days as

384 described previously (33) and arranged in a randomized block design. The shoots or leaf
385 primordia were frozen in liquid nitrogen just after sampling, and then stored at –80°C
386 until use for DNA and RNA extractions. All F2 plants were grown in a field in the
387 University of California, Davis with an interplant spacing of 30 x 30 cm^2 for
388 transplanting.
389
390 **Morphological Observations**
391 For morphological observations and collecting tissues for RNA extractions, shoots and
392 leaves were dissected under the dissection microscopes (Discovery.V12; ZEISS). To
393 determine the vascular density of leaves, the 6th leaves were used and cleared using an
394 ethanol and 50 % bleach following Rowland *et al.* (2019). The samples were then
395 photographed under the microscopes (ECLIPSE E600; Nikon), and vascular length per
396 unit area was determined using ImageJ software (http://rsb.info.nih.gov/ij/) (n = 4). Leaf
397 complexity was determined by counting the numbers of leaflets and intercalary leaflets
398 on a fully developed leaf (n = 29). Traditional leaf shape analysis was performed
399 following (34). Leaf complexity and leaflet shapes were analyzed for leaves collected

400 from the chamber. The leaf complexity measures included all leaflets present on the
401 leaf. After complexity was obtained the primary leaflets were removed and used for
402 imaging and analysis of shape and size. The intercalary and secondary/tertiary leaflets
403 were not used for shape analysis due to their smaller size and irregular shapes. The
404 binary images were then processed in R using MOMOCS, a shape analysis package
405 (35).
406

407 **Phylogenetic Analyses of Isolated Genes**

408 The predicted amino acid sequences of isolated genes were aligned using ClustalW and
409 readjusted manually. Phylogenetic trees were reconstructed using MEGA6 (36) using
410 the neighbor-joining method (37) (38). Bootstrap values were derived from 1000
411 replicate runs. The ML phylogenetic tree with the highest log likelihood is shown.
412 Initial trees for the heuristic search were obtained automatically: Neighbor-Join and
413 BioNJ algorithms were applied to a matrix of pairwise distances estimated with MCL,
414 and then the topology with a superior log likelihood value was selected. The tree is
415 drawn to scale, with branch lengths measured in the number of substitutions per site.

Whole-mount In Situ Hybridization

Portions of genes isolated in pCR 2.1 (Invitrogen) were amplified by PCR using the universal primers M13_F (-20) (GTAAAACGACGGCCAC) and M13_R (CAGGAAACAGCTATGAG). The amplified fragments were then used to produce digoxigenin (DIG)-labeled sense and antisense RNA probes using a DIG RNA Labeling Kit (Roche). Whole-mount in situ hybridization was performed following (39). Shoots were fixed in 1x PBST containing 4% (w/v) paraformaldehyde, 1% (w/v) glutaraldehyde. Fixed samples were dehydrated in an ethanol series. The dehydrated samples were stored in 100% methanol at –20°C until use for the experiment. DIG-labeled sense and antisense RNA probes were synthesized with T7 RNA polymerase (Roche). For immunological detection, the samples were incubated in detection buffer containing NBT-BCIP (Roche) at 25 °C for several hours or 4°C overnight. Photographs were taken using an ECLIPSE E600 (Nikon). The experiments were performed at least three times.

Quantitative Real-Time PCR

Total RNA was extracted from leaf primordia of plants grown for a month and used to synthesize cDNA, as described above. The quantitative RT-PCR analysis was conducted using the following gene-specific primer pairs: Tkn1_RT_F and Tkn1_RT_R; SlWOX1_RT_F and SlWOX1_RT_R; and SlGAPDH_RT_F and SlGAPDH_RT_R (Supplemental Table 7). Real-time PCR amplification was performed using the iTaq Universal SYBR (BIO-RAD) in a iQ5 Real-Time PCR Detection System (BIO-RAD). Experiments were performed in triplicate from three independent tissue RNA extractions. Expression was normalized to the Sl *GAPDH* control.

Deep learning-based nonlinear PCA

For nonlinear PCA on image data, we used leaflet images from M82, *bip3*, and SiFT for the analysis (4th leaf; $N < 55$) and adopted a pre-trained neural network with the ImageNet dataset, VGG19 (40), as feature extractor. Instead of the original scanned images, binary silhouette images were fed into the network in order to avoid the effects of non-morphogenetic features such as leaf color. We extracted images features from an intermediate layer, "block4_pool" through Keras 2.3.1 library (https://keras.io). Then the

448 linear PCA was applied on the image features. We performed no training of the neural
449 network with our data, so that the feature extraction was completely agnostic on which
450 genotypes the leaves came from.

451

452 **DNA-Seq and RNA-Seq Library Preparation and Sequencing**

453 DNA-Seq libraries for BSA were prepared following (41). DNA was extracted using
454 GeneJET Plant Genomic DNA Purification Mini Kit (Thermo Scientific, Waltham, MA,
455 USA) from plants grown for a month. DNA-Seq libraries for phylogenic analysis were
456 prepared based on BrAD-seq (42) with the following modifications: After DNA
457 fragmentation with Covaris E220 (Covaris, Inc. Woburn, MA, USA), the fragmented
458 DNA was end-repaired, A-tailed, and adapter ligated with Y-adapter. Enrichment PCR
459 was then performed with the adapter ligated product as described Townsley et al., 2015.
460 After final library cleanup with AMPure beads (Beckman Coulter, Brea, CA, USA),
461 RNA-Seq libraries were prepared following (42) from four biological replicates of
462 proximal and distal regions of leaf primordia at four developmental stages (meristem +
463 P1-P3; P4; P5). DNA-Seq libraries were sequenced at Novogene (Novogene Inc.

464 Sacramento, CA, USA). RNA-Seq libraries were sequenced at the University of
465 California Berkeley Vincent J. Coates Genomics Sequencing Laboratory using the HiSeq
466 2000 platform (Illumina Inc. San Diego, CA, USA).
467
468 **SNP calling and Allele frequency analysis with DNA-seq data and Phylogenetic**
469 **analysis with Whole genome sequencing data**
470 To detect SNPs in SiFT genome and perform phylogenetic analysis, all variants detected
471 by CLC Genomics Workbench 11.0 (CLC Bio, a QIAGEN Company, Aarhus, Denmark).
472 After read mapping and local realignment, Fixed Ploidy Variant Detection function was
473 used for calculation of allele frequency. For phylogenetic analysis, the data were exported
474 as vcf files. The SNPRelate package for R (43) was used to determine the variant positions
475 that overlapped between cultivars and then all sequences combined into a single gds file.
476 This file was run through SNPhylo (44) with the following parameters: The linkage
477 disequilibrium was set to 1.0, as we wanted to exclude as few variants as possible based
478 on this factor, minor allele frequency was set to 0.05, and the Missing rate was set to 0.1.
479 One thousand bootstraps were performed for confidence intervals and significance. *S.*

480 *pimpinellifolium* was used as the out group. The output bootstrapped tree was displayed
481 in MEGA6 (36).
482
483 **Mapping, Normalization, and Network analysis with RNA-Seq data**
484 The 50 bp single-end sequence reads obtained were quality trimmed and parsed to
485 individual libraries using custom Perl scripts. All reads were mapped to the ITAG2.4
486 genome build (downloadable from http://solgenomics.net/itag/release/2.4/list_files)
487 using RSEM/eXpress with the default parameters (45). The uniquely mapped read data
488 was normalized using the Bioconductor package EdgeR ver. 2.11 with the trimmed
489 mean of M-values method. Bioinformatics and statistical analyses were performed on
490 the iPLANT (Cyverse) Atmosphere cloud server (46). Gene Co-expression network
491 analysis was performed following (14) by using the R script. The R script for RNA-Seq
492 gene coexpression network analysis deposited on GitHub (Link:
493 https://github.com/Hokuto-GH/gene-coexpression-network-script). For GO enrichment
494 analysis, we used GENEONTOLOGY enrichment analysis tools
495 (http://geneontology.org/docs/go-enrichment-analysis/). DiffCorr analysis was

performed following (15). The normalized count data from M82 and SiFT was used for the analysis. DiffCorr genes were then analyzed to identify the most different gene between two genotypes at a 0.005 FDR cut-off. To analyze and visualize the DiffCorr genes, Cytoscape was used (https://cytoscape.org/). The number of Edges of each DiffCorr gene was calculated by analyze network function in the Cytoscape. Then, the numbers were compared to figure out the most different gene between two genotypes.

CRISPR–Cas9 mutagenesis and plant transformation

CRISPR–Cas9 mutagenesis and generation of transgenic plants was performed following REF. Guide (g) RNAs for *SF/SlWOX1* (Solyc03g118770) were designed using the CCtop (https://crispr.cos.uni-heidelberg.de/help.html) and two gRNAs were designed (Fig. 5). Vectors were assembled using the Golden Gate cloning system as described (47). Final binary vector was transformed into the tomato cultivars M82 by *Agrobacterium tumefaciens*-mediated transformation. The transformation was performed at the Ralph M. Parsons Foundation Plant Transformation Facility (University of California, Davis). The first-generation (T_0) transgenics were genotyped

using GT-seq following (48). It revealed a single nucleotide substitution (C to A) in gRNA2 (g2) region. Unfortunately, there were no T_0 transgenics having mutation in the region of gRNA1 (g1) region. After the genotyping and self-pollination in the green house, we obtained T_1 plants having mutated *sf/slwox1* gene. First, we screened those plants by leaf phenotypes because *wox1* mutants must have narrower leaflets compared to WT based on previous studies with various kinds of plant species. Then we did genotyping by sequencing to confirm whether each individual has the *sf/slwox1* mutation or not.

PhyloNetwork Analyses

To perform phylogenetic analysis, all SNPs detected by CLC Genomics Workbench 11.0 (CLC Bio, a QIAGEN Company, Aarhus, Denmark) from whole genome sequencing obtained from the 360 genomes project (49) were exported as a vcf file. The VCFtools package (50) was to convert vcf files to fasta files and these sequences were aligned using ClustalW. All aligned SNPs from the two megabase region surrounding the BIP gene for 32 cultivars were run through the TICR pipeline (51). They were then

528 analyzed using PhyloNetworks with default settings with the following exceptions: the
529 number of runs was set to 10 and Nfail was set to 10. After the hybrid network was
530 obtained bootstrap analysis was done in PhyloNetworks using default settings with the
531 following exceptions: Runs was set to 10 and Nfail was set to 10. These adjustments
532 were made to decrease processing time. The bootstrapped tree was output in
533 Dendroscope (52).
534

535 **Statistical analysis**

536 All statistical analyses were performed using JMP (JMP Pro 14.0.0, 2018) software. To
537 determine statistical significance, measurements were modeled using general linear
538 regression model and tested by a one-way ANOVA followed by Tukey's honestly
539 significant difference, if necessary.
540

541 **Data availability**

542 All data is available in the main text or the supplementary materials. All DNA-Seq and
543 RNA-Seq raw data are deposited on DDBJ DRA009167- 009182 (BioProject:

PRJDB8552). Source Data files for all main and supplementary figures are available in the online version of the paper. All additional data sets are available from the corresponding author on request.

Acknowledgements

This work was supported by grants from the USDA NIFA (2014-67013-21700), NSF; IOS (1558900), and JSPS KAKENHI (19K23742 and 20K06682 to H.N. and 19H05670 to Y.K.). Hokuto Nakayama was a recipient of a JSPS Fellowship (13J00161). We are grateful to Lauren Hughes for generating the initial cross between SiFT and M82, Donnelly West for the F2 seeds, and Amber Flores for helping with field measurements.

Author contributions

H.N. initiated the project. N.R.S. supervised the project. H.N. and N.R.S. designed experiments. H.N. performed the majority of the experiments and analyses and prepared

559 figures. S.D.R., Z.C., K.Z., J.C., and Y.K. performed experiments. H.N. and S.D.R.

560 analyzed the data. H.N. and N.R.S. wrote the paper with the input from all authors.

561

562 **Corresponding Author**

563 Correspondence to Neelima R. Sinha

564

565 **Competing interests**

566 The authors declare that they have no competing interests.

567

Figure legends

Figure 1. Gross morphology and development in M82 and SiFT leaves.
Top view of shoots (A), and mature leaf morphology (B). The 4th leaves were used for (B). Left: M82; right: SiFT. (C) Comparison of leaf complexity ($N = 14$). $p = 0.0000059$ (Welch's t-test). (D) Comparison of leaf morphology of M82 (upper) and SiFT (lower). All silhouettes are based on photographic images. The youngest leaf is at the right and the oldest (cotyledons) is at the left. (E) Developmental trajectory of M82 and SiFT leaf primordia. The 4th and 5th leaves were represented. (F) Cleared terminal leaflet images of M82 and SiFT. Bars = 2 cm in (A), (B) and (D), 100 μm in (E), and 1 mm in (F).

Figure 2. Identification of the causative mutation for the *BIPINNATA* gene.
(A) Top: allele frequency between different pools of segregating populations (red: high complexity pool; blue: low complexity pool) is shown for chromosome 2 (Chr 2). Middle: variants (SNPs and indels) in SiFT from whole genome sequencing data. Each dot indicates variant position on Chr 2. Bottom: deleterious mutations in SiFT indicated from PROVEAN. Each vertical line indicates deleterious mutation on Chr 2. All panels (top, middle, and bottom) show the same scale on Chr 2. (B) Exon and intron structure of *BIPINNATA* (*BIP*). *BIP* gene contains five exons. SiFT contains an 1 bp deletion, which leads truncated protein and an amino acid change in the highly conserved amino acid of homeodomain (C).

Figure 3. *bipinnata* leaf phenotypes.
(A) Mature leaf morphology. The 4th leaves were used. Left: SiFT; right: *bip3*. (B) Comparison of leaf complexity ($N = 14$). (C) Leaf development of *bip3* at P4 stage. (D) Whole mount *in situ* localization of *BIP* transcripts in M82. Left: sense probe; Right: antisense probe. (E) Expression level of *Tkn1* in leaf primordia ($N = 3$). $p = 0.00107513$ (Welch's *t*-test). (F) Deep learning-based nonlinear PCA with leaflet shapes ($N < 55$). Blue: M82, pink: SiFT, and orange: *bip3*. (G) Comparison of terminal leaflet morphology. Left; leaflet morphology used for leaf shape analysis. All silhouettes are

based on scanned images. Right; results of leaf width measurement with terminal leaflets. $p = 8.8 \times 10^{-8}$ (Welch's *t*-test). (H) Cleared terminal leaflet images of M82, SiFT and *bip3*. (I) Vascular density per unit area. The data was assessed using pair-wise comparisons with Tukey-Kramer HSD test. Bars = 2 cm in (A), 100 μm in (C), 500 μm in (D), 1 cm in (G), and 1 mm in (H).

Figure 4. Gene co-expression network analysis with M82 and SiFT RNA-seq data. (A) Gene co-expression networks for genes involved in leaf development. Each node represents genes. Only nodes with at least one edge are represented. Left: M82; right: SiFT. (B) An overview of the enriched GO terms visualized by bubble plot. The analysis was performed by the community in each network (C1 and C2). Each bubble represents a GO term and only GO terms with higher Fold enrichment (>50) are represented. For full result of the GO enrichment analysis, please see Supplementary Table 3. (C) A profile of 160 DiffCorr genes. The plot on the top: the number of differential correlations of each DiffCorr gene. A higher number means more difference between M82 and SiFT networks. The heat map on the bottom: a comparison of expression level of each DiffCorr gene between M82 and SiFT. Each expression level is shown as a blue-to-yellow-colored scale. The 160 DiffCorr genes were sorted by the number of differential correlations (Left: low; right: high). The position of each gene is the same between the top and bottom panels. (D) The Sl *WOX1* gene network from M82 shown in (A). This network is consisted of genes only showing a direct connection to the Sl *WOX1*. (E) Expression level of Sl *WOX1* in leaf primordia ($N = 4$). $p = 0.011$ (Welch's *t*-test). (F and G) Whole mount *in situ* localization of Sl *WOX1* transcripts in M82. (F) Leaf primordia. (G) Leaflet primordia. Left: sense probe; right: antisense probe in each panel. Bars = 100 μm in (F) and (G).

Figure 5. *solanifolia*/*slwox1* leaf phenotypes. (A) Exon and intron structure of *SF*/*SlWOX1*. The tomato *SF*/*SlWOX1* gene contains four exons. (B) Mature leaf morphology of *sf*/*slwox1* mutants. The 4th leaves were used. (C) Comparison of aspect ratio (width/length) and width of terminal leaflet ($N = 10$). Letters indicate significance groups; samples with the same letters are not significantly

633 different. All data were assessed using pair-wise comparisons with Tukey-Kramer HSD
634 test. (D) Comparison of vascular density. Cleared terminal leaflet images. Bars = 2 cm
635 in (B) and 1 mm in (D).
636
637
638 **Figure 6. *bip sf* double mutant leaf phenotypes.**
639 (A) Mature leaf morphology of *bip3* e1862 double mutant. From left to right: *bip3*,
640 e1862, and *bip3* e1862 double mutant. The 4th leaves were used. (B) Close-up view of a
641 secondary leaflet on a 4th leaf in the double mutant shown in (A). (C) Comparison of
642 secondary leaflets on matured 6th leaf from 60 days old seedlings. (D) Cleared terminal
643 leaflet images of *bip3*, e1862, and *bip3* e1862 double mutant. (E) A schematic model
644 for leaf development in SiFT. Bars = 2 cm in (A) and (C), 1 cm in (B), and 1mm = in
645 (D).
646
647
648 **Figure 7. Reconstruction of breeding history and comparison of SNPs data.**
649 (A) PhyloNetwork with sequences around the *BIP* locus on chromosome 2. The
650 network describes various biological processes such as hybridization or introgression
651 (Blue lines). The bootstrap values are indicated on branches (only those more than 50%
652 are indicated on the tree). (B) Magnified view of the network shown in (A) focusing on
653 SiFT. Comparison of SNPs data around *BIP* locus (Solyc02g089940) with heirloom
654 tomatoes (C) and a wild species (D). Each vertical black line indicates a SNP.
655
656
657 **Figure 8. Breeding history and diversification of leaf shape in cultivated Toamto.**
658 Simplified phylogeny presented in Fig. 7 with leaf morphologies. Boxes indicate
659 presumed key events during evolution. See text for details.
660
661
662

References

1. J. Diamond, Evolution, consequences and future of plant and animal domestication. *Nature* **418**, 700-707 (2002).
2. R. S. Meyer, M. D. Purugganan, Evolution of crop species: genetics of domestication and diversification. *Nat Rev Genet* **14**, 840-852 (2013).
3. C. Darwin, *The variation of animals and plants under domestication* (O. Judd, 1868), vol. 2.
4. J. A. Labate *et al.*, "Tomato" in Vegetables, C. Kole, Ed. (Springer Berlin Heidelberg, Berlin, Heidelberg, 2007), 10.1007/978-3-540-34536-7_1, pp. 1-125.
5. G. Bauchet, M. Causse, "Genetic diversity in tomato (Solanum lycopersicum) and its wild relatives" in Genetic diversity in plants. (InTech, 2012).
6. A. Goldman, V. Schrager (2008) The Heirloom Tomato: From Garden to Table. (Bloomsbury Publishing: New York).
7. D. Tieman *et al.*, A chemical genetic roadmap to improved tomato flavor. *Science* **355**, 391-394 (2017).
8. S. Kessler, M. Kim, T. Pham, N. Weber, N. Sinha, Mutations altering leaf morphology in tomato. *International journal of plant sciences* **162**, 475-492 (2001).
9. Y. Choi, G. E. Sims, S. Murphy, J. R. Miller, A. P. Chan, Predicting the functional effect of amino acid substitutions and indels. *PLoS One* **7**, e46688 (2012).
10. S. Kimura, D. Koenig, J. Kang, F. Y. Yoong, N. Sinha, Natural variation in leaf morphology results from mutation of a novel KNOX gene. *Curr Biol* **18**, 672-677 (2008).
11. R. Kumar *et al.*, The Arabidopsis BEL1-LIKE HOMEODOMAIN proteins SAW1 and SAW2 act redundantly to regulate KNOX expression spatially in leaf margins. *Plant Cell* **19**, 2719-2735 (2007).
12. B. J. Janssen, L. Lund, N. Sinha, Overexpression of a homeobox gene, LeT6, reveals indeterminate features in the tomato compound leaf. *Plant Physiol* **117**, 771-786 (1998).
13. P. Tieri *et al.*, Network Inference and Reconstruction in Bioinformatics. (2019).
14. Y. Ichihashi *et al.*, Evolutionary developmental transcriptomics reveals a gene network module regulating interspecific diversity in plant leaf shape. *Proceedings of the National Academy of Sciences of the United States of America* **111**, E2616-2621 (2014).
15. A. Fukushima, DiffCorr: an R package to analyze and visualize differential correlations in biological networks. *Gene* **518**, 209-214 (2013).

16. M. Nakata *et al.*, Roles of the middle domain-specific WUSCHEL-RELATED HOMEOBOX genes in early development of leaves in Arabidopsis. *Plant Cell* **24**, 519-535 (2012).

17. M. Tadege *et al.*, STENOFOLIA regulates blade outgrowth and leaf vascular patterning in Medicago truncatula and Nicotiana sylvestris. *Plant Cell* **23**, 2125-2142 (2011).

18. K. C. Sekhar, V. Sawhney, Leaf development in the normal and solanifolia mutant of tomato (Lycopersicon esculentum). *American journal of botany* **77**, 46-53 (1990).

19. H. Wang *et al.*, Overexpression of the WOX gene STENOFOLIA improves biomass yield and sugar release in transgenic grasses and display altered cytokinin homeostasis. *PLoS genetics* **13**, e1006649 (2017).

20. C. Guan *et al.*, Spatial Auxin Signaling Controls Leaf Flattening in Arabidopsis. *Curr Biol* **27**, 2940-2950.e2944 (2017).

21. T. Yifhar *et al.*, Failure of the tomato trans-acting short interfering RNA program to regulate AUXIN RESPONSE FACTOR3 and ARF4 underlies the wiry leaf syndrome. *Plant Cell* **24**, 3575-3589 (2012).

22. S.-Y. Hong, O.-K. Kim, S.-G. Kim, M.-S. Yang, C.-M. Park, Nuclear import and DNA binding of the ZHD5 transcription factor is modulated by a competitive peptide inhibitor in Arabidopsis. *Journal of Biological Chemistry* **286**, 1659-1668 (2011).

23. S. Soyk *et al.*, Duplication of a domestication locus neutralized a cryptic variant that caused a breeding barrier in tomato. *Nature plants* **5**, 471-479 (2019).

24. C. Solís-Lemus, P. Bastide, C. Ané, PhyloNetworks: A Package for Phylogenetic Networks. *Molecular Biology and Evolution* **34**, 3292-3298 (2017).

25. E. Shani *et al.*, Stage-specific regulation of Solanum lycopersicum leaf maturation by class 1 KNOTTED1-LIKE HOMEOBOX proteins. *Plant Cell* **21**, 3078-3092 (2009).

26. M. G. Sawchuk, A. Edgar, E. Scarpella, Patterning of leaf vein networks by convergent auxin transport pathways. *PLoS genetics* **9**, e1003294 (2013).

27. D. E. Soltis *et al.*, The Amborella genome: an evolutionary reference for plant biology. *Genome biology* **9**, 402 (2008).

28. F. Zhang *et al.*, STENOFOLIA recruits TOPLESS to repress ASYMMETRIC LEAVES2 at the leaf margin and promote leaf blade outgrowth in Medicago truncatula. *Plant Cell* **26**, 650-664 (2014).

29. D. Kierzkowski *et al.*, A Growth-Based Framework for Leaf Shape Development and Diversity. *Cell* **177**, 1405-1418.e1417 (2019).

30. S. D. Rowland *et al.*, Leaf shape is a predictor of fruit quality and cultivar performance in

728 tomato. *The New phytologist* 10.1111/nph.16403 (2019).

729 31. D. H. Chitwood *et al.*, Resolving distinct genetic regulators of tomato leaf shape within a
730 heteroblastic and ontogenetic context. *Plant Cell* **26**, 3616-3629 (2014).

731 32. N. Menda, Y. Semel, D. Peled, Y. Eshed, D. Zamir, In silico screening of a saturated
732 mutation library of tomato. *The Plant journal : for cell and molecular biology* **38**, 861-872
733 (2004).

734 33. S. Kimura, N. Sinha, How to grow tomatoes. *CSH protocols* **2008**, pdb.prot5081 (2008).

735 34. D. H. Chitwood *et al.*, A modern ampelography: a genetic basis for leaf shape and venation
736 patterning in grape. *Plant Physiol* **164**, 259-272 (2014).

737 35. V. Bonhomme, S. Picq, C. Gaucherel, J. Claude, Momocs: outline analysis using R. *J Stat*
738 *Softw* **56**, 1-24 (2014).

739 36. K. Tamura, G. Stecher, D. Peterson, A. Filipski, S. Kumar, MEGA6: Molecular Evolutionary
740 Genetics Analysis version 6.0. *Mol Biol Evol* **30**, 2725-2729 (2013).

741 37. N. Saitou, M. Nei, The neighbor-joining method: a new method for reconstructing
742 phylogenetic trees. *Mol Biol Evol* **4**, 406-425 (1987).

743 38. K. Tamura, M. Nei, Estimation of the number of nucleotide substitutions in the control
744 region of mitochondrial DNA in humans and chimpanzees. *Mol Biol Evol* **10**, 512-526 (1993).

745 39. F. Rozier, V. Mirabet, T. Vernoux, P. Das, Analysis of 3D gene expression patterns in plants
746 using whole-mount RNA in situ hybridization. *Nature protocols* **9**, 2464-2475 (2014).

747 40. K. Simonyan, A. Zisserman, Very deep convolutional networks for large-scale image
748 recognition. *arXiv preprint arXiv:1409.1556* (2014).

749 41. B. A. Rowan, D. K. Seymour, E. Chae, D. S. Lundberg, D. Weigel, Methods for Genotyping-
750 by-Sequencing. *Methods in molecular biology (Clifton, N.J.)* **1492**, 221-242 (2017).

751 42. B. T. Townsley, M. F. Covington, Y. Ichihashi, K. Zumstein, N. R. Sinha, BrAD-seq: Breath
752 Adapter Directional sequencing: a streamlined, ultra-simple and fast library preparation
753 protocol for strand specific mRNA library construction. *Frontiers in plant science* **6**, 366
754 (2015).

755 43. X. Zheng *et al.*, A high-performance computing toolset for relatedness and principal
756 component analysis of SNP data. *Bioinformatics (Oxford, England)* **28**, 3326-3328 (2012).

757 44. T. H. Lee, H. Guo, X. Wang, C. Kim, A. H. Paterson, SNPhylo: a pipeline to construct a
758 phylogenetic tree from huge SNP data. *BMC Genomics* **15**, 162 (2014).

759 45. B. Li, C. N. Dewey, RSEM: accurate transcript quantification from RNA-Seq data with or
760 without a reference genome. *BMC bioinformatics* **12**, 323 (2011).

761 46. S. A. Goff *et al.*, The iPlant Collaborative: Cyberinfrastructure for Plant Biology. *Frontiers*
762 *in plant science* **2**, 34 (2011).
763 47. S. Werner, C. Engler, E. Weber, R. Gruetzner, S. Marillonnet, Fast track assembly of
764 multigene constructs using Golden Gate cloning and the MoClo system. *Bioengineered bugs*
765 **3**, 38-43 (2012).
766 48. N. R. Campbell, S. A. Harmon, S. R. Narum, Genotyping-in-Thousands by sequencing (GT-
767 seq): A cost effective SNP genotyping method based on custom amplicon sequencing.
768 *Molecular ecology resources* **15**, 855-867 (2015).
769 49. T. Lin *et al.*, Genomic analyses provide insights into the history of tomato breeding. *Nature*
770 *genetics* **46**, 1220-1226 (2014).
771 50. P. Danecek *et al.*, The variant call format and VCFtools. *Bioinformatics (Oxford, England)*
772 **27**, 2156-2158 (2011).
773 51. N. W. Stenz, B. Larget, D. A. Baum, C. Ané, Exploring Tree-Like and Non-Tree-Like
774 Patterns Using Genome Sequences: An Example Using the Inbreeding Plant Species
775 Arabidopsis thaliana (L.) Heynh. *Syst Biol* **64**, 809-823 (2015).
776 52. D. H. Huson, C. Scornavacca, Dendroscope 3: an interactive tool for rooted phylogenetic
777 trees and networks. *Syst Biol* **61**, 1061-1067 (2012).

778

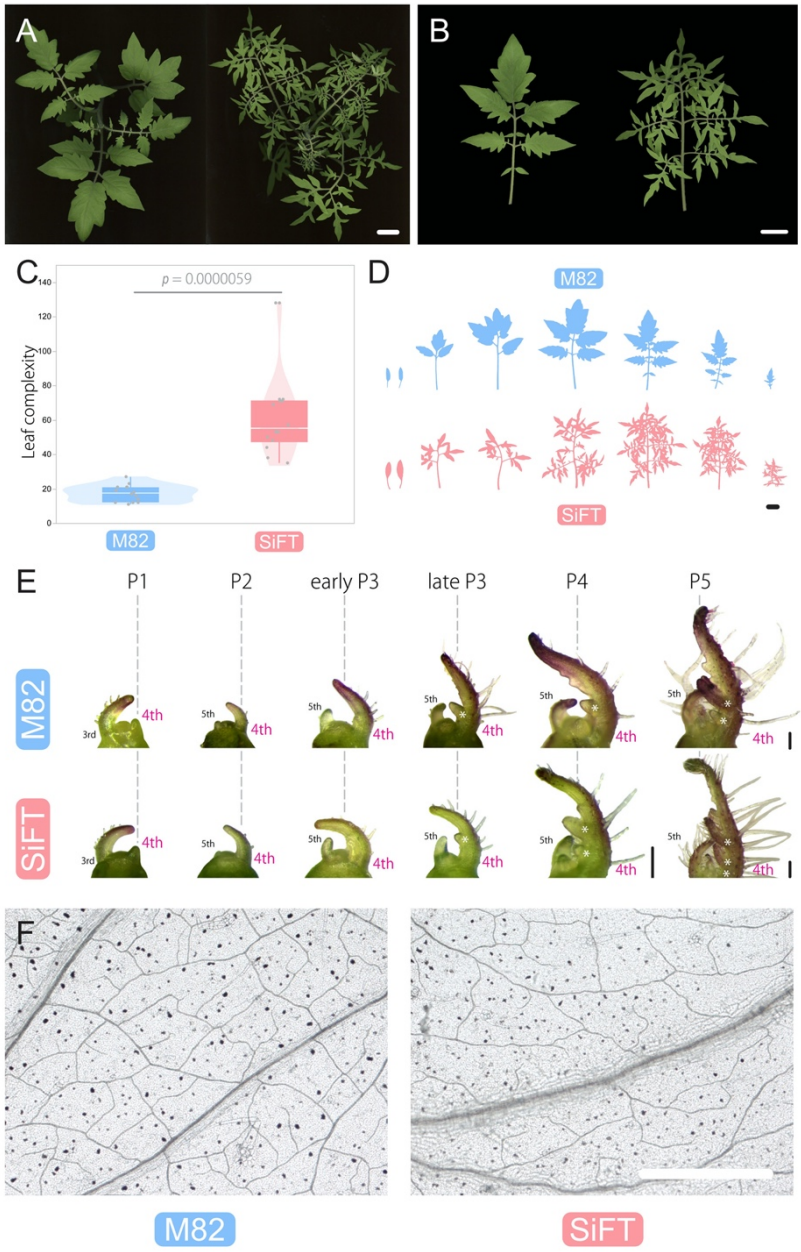

Figure 1. Gross morphology and development in M82 and SiFT leaves.

Top view of shoots (A), and mature leaf morphology (B). The 4th leaves were used for (B). Left: M82; right: SiFT. (C) Comparison of leaf complexity ($N = 14$). $p = 0.0000059$ (Welch's t-test). (D) Comparison of leaf morphology of M82 (upper) and SiFT (lower). All silhouettes are based on photographic images. The youngest leaf is at the right and the oldest (cotyledons) is at the left. (E) Developmental trajectory of M82 and SiFT leaf primordia. The 4th and 5th leaves were represented. (F) Cleared terminal leaflet images of M82 and SiFT. Bars = 2 cm in (A), (B) and (D), 100 μm in (E), and 1 mm in (F).

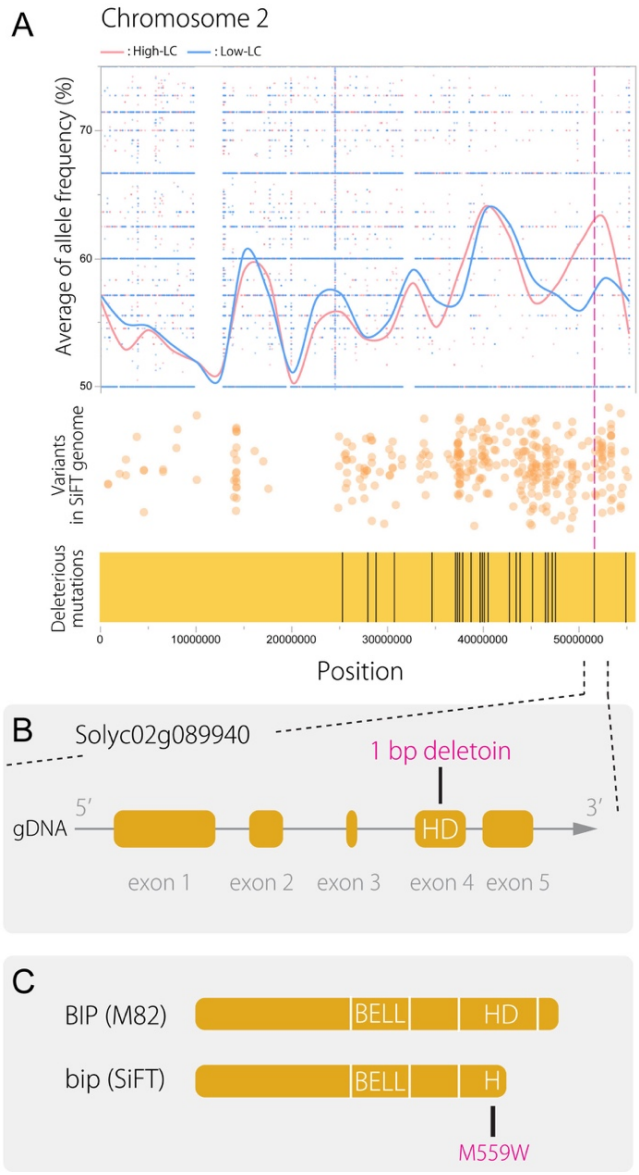

Figure 2. Identification of the causative mutation for the *BIPINNATA* gene.

(A) Top: allele frequency between different pools of segregating populations (red: high complexity pool; blue: low complexity pool) is shown for chromosome 2 (Chr 2). Middle: variants (SNPs and indels) in SiFT from whole genome sequencing data. Each dot indicates variant position on Chr 2. Bottom: deleterious mutations in SiFT indicated from PROVEAN. Each vertical line indicates deleterious mutation on Chr 2. All panels (top, middle, and bottom) show the same scale on Chr 2. (B) Exon and intron structure of *BIPINNATA* (*BIP*). *BIP* gene contains five exons. SiFT contains an 1 bp deletion, which leads truncated protein and an amino acid change in the highly conserved amino acid of homeodomain (C).

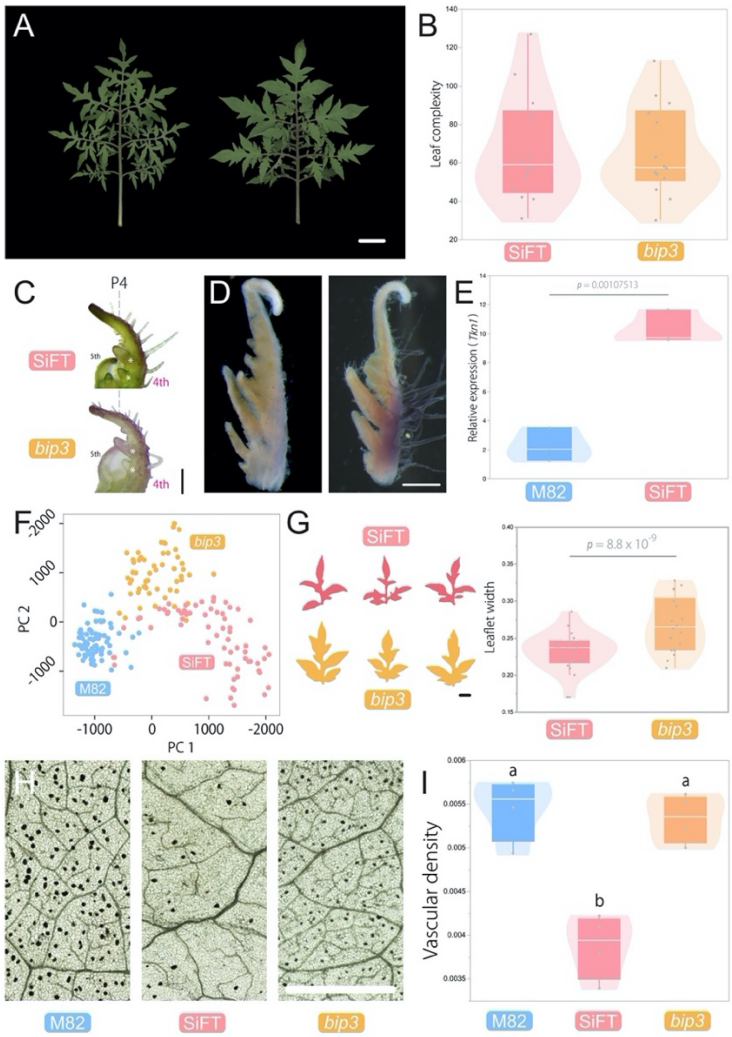

Figure 3. *bipinnata* leaf phenotypes.

(A) Mature leaf morphology. The 4th leaves were used. Left: SiFT; right: *bip3*. (B) Comparison of leaf complexity ($N = 14$). (C) Leaf development of *bip3* at P4 stage. (D) Whole mount *in situ* localization of *BIP* transcripts in M82. Left: sense probe; Right: antisense probe. (E) Expression level of *Tkn1* in leaf primordia ($N = 3$). $p = 0.00107513$ (Welch's *t*-test). (F) Deep learning-based nonlinear PCA with leaflet shapes ($N < 55$). Blue: M82, pink: SiFT, and orange: *bip3*. (G) Comparison of terminal leaflet morphology. Left; leaflet morphology used for leaf shape analysis. All silhouettes are based on scanned images. Right; results of leaf width measurement with terminal leaflets. $p = 8.8 \times 10^{-8}$ (Welch's *t*-test). (H) Cleared terminal leaflet images of M82, SiFT and *bip3*. (I) Vascular density per unit area. The data was assessed using pair-wise comparisons with Tukey-Kramer HSD test. Bars = 2 cm in (A), 100 μm in (C), 500 μm in (D), 1 cm in (G), and 1 mm in (H).

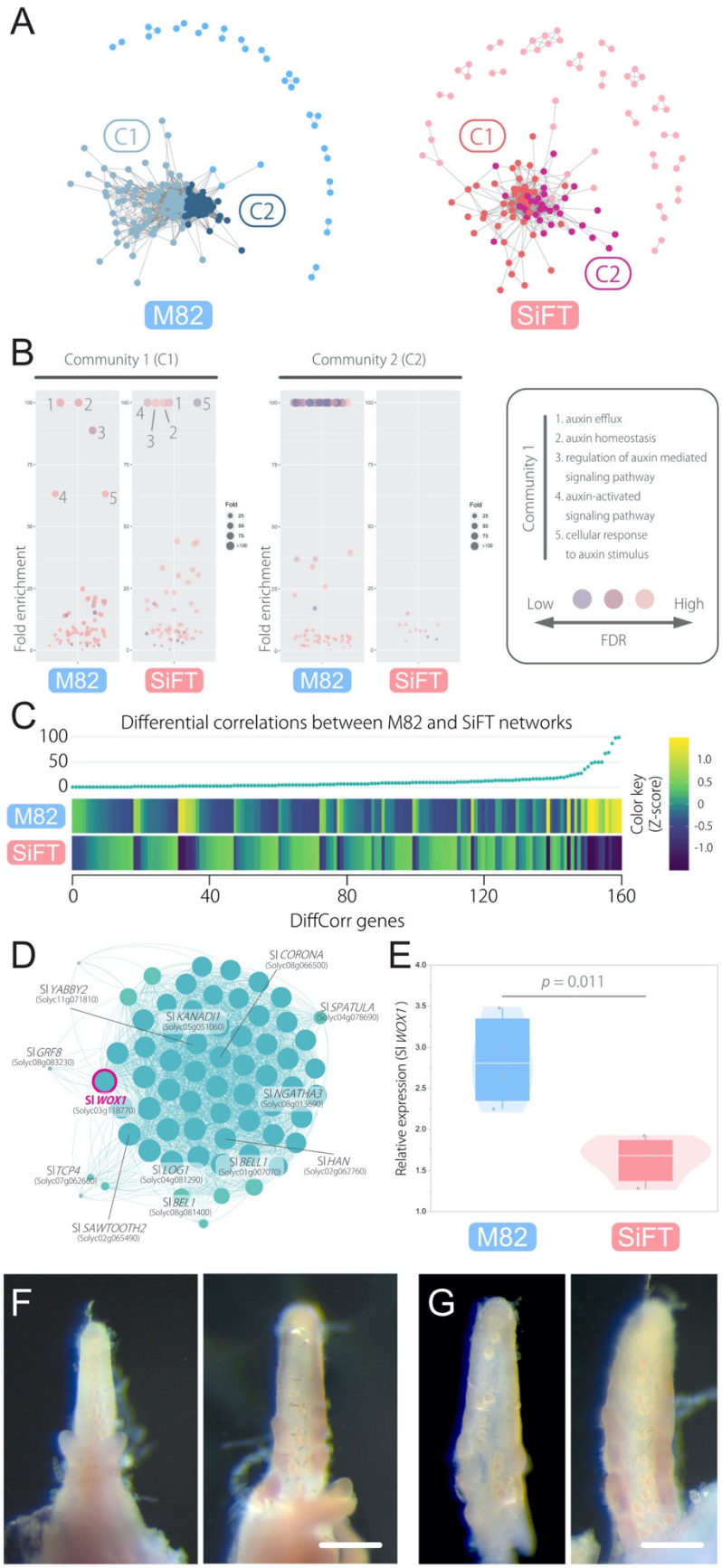

Figure 4. Gene co-expression network analysis with M82 and SiFT RNA-seq data. (A) Gene co-expression networks for genes involved in leaf development. Each node represents genes. Only nodes with at least one edge are represented. Left: M82; right: SiFT. (B) An overview of the enriched GO terms visualized by bubble plot. The analysis was performed by the community in each network (C1 and C2). Each bubble represents a GO term and only GO terms with higher Fold enrichment (>50) are represented. For full result of the GO enrichment analysis, please see Supplementary Table 3. (C) A profile of 160 DiffCorr genes. The plot on the top: the number of differential correlations of each DiffCorr gene. A higher number means more difference between M82 and SiFT networks. The heat map on the bottom: a comparison of expression level of each DiffCorr gene between M82 and SiFT. Each expression level is shown as a blue-to-yellow-colored scale. The 160 DiffCorr genes were sorted by the number of differential correlations (Left: low; right: high). The position of each gene is the same between the top and bottom panels. (D) The Sl *WOX1* gene network from M82 shown in (A). This network is consisted of genes only showing a direct connection to the Sl *WOX1*. (E) Expression level of Sl *WOX1* in leaf primordia ($N = 4$). $p = 0.011$ (Welch's t-test). (F and G) Whole mount *in situ* localization of Sl *WOX1* transcripts in M82. (F) Leaf primordia. (G) Leaflet primordia. Left: sense probe; right: antisense probe in each panel. Bars = 100 μm in (F) and (G).

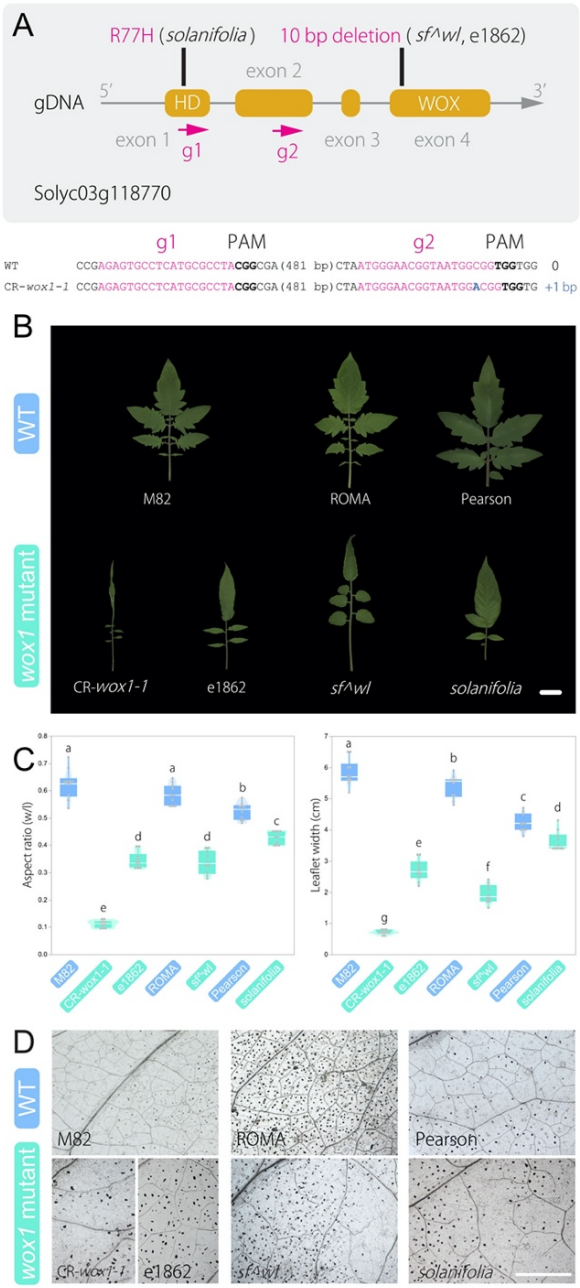

(A) Exon and intron structure of *SF*/*SlWOX1*. The tomato *SF*/*SlWOX1* gene contains four exons. (B) Mature leaf morphology of *sf*/*slwox1* mutants. The 4th leaves were used. (C) Comparison of aspect ratio (width/length) and width of terminal leaflet ($N = 10$). Letters indicate significance groups; samples with the same letters are not significantly different. All data were assessed using pair-wise comparisons with Tukey-Kramer HSD test. (D) Comparison of vascular density. Cleared terminal leaflet images. Bars = 2 cm in (B) and 1 mm in (D).

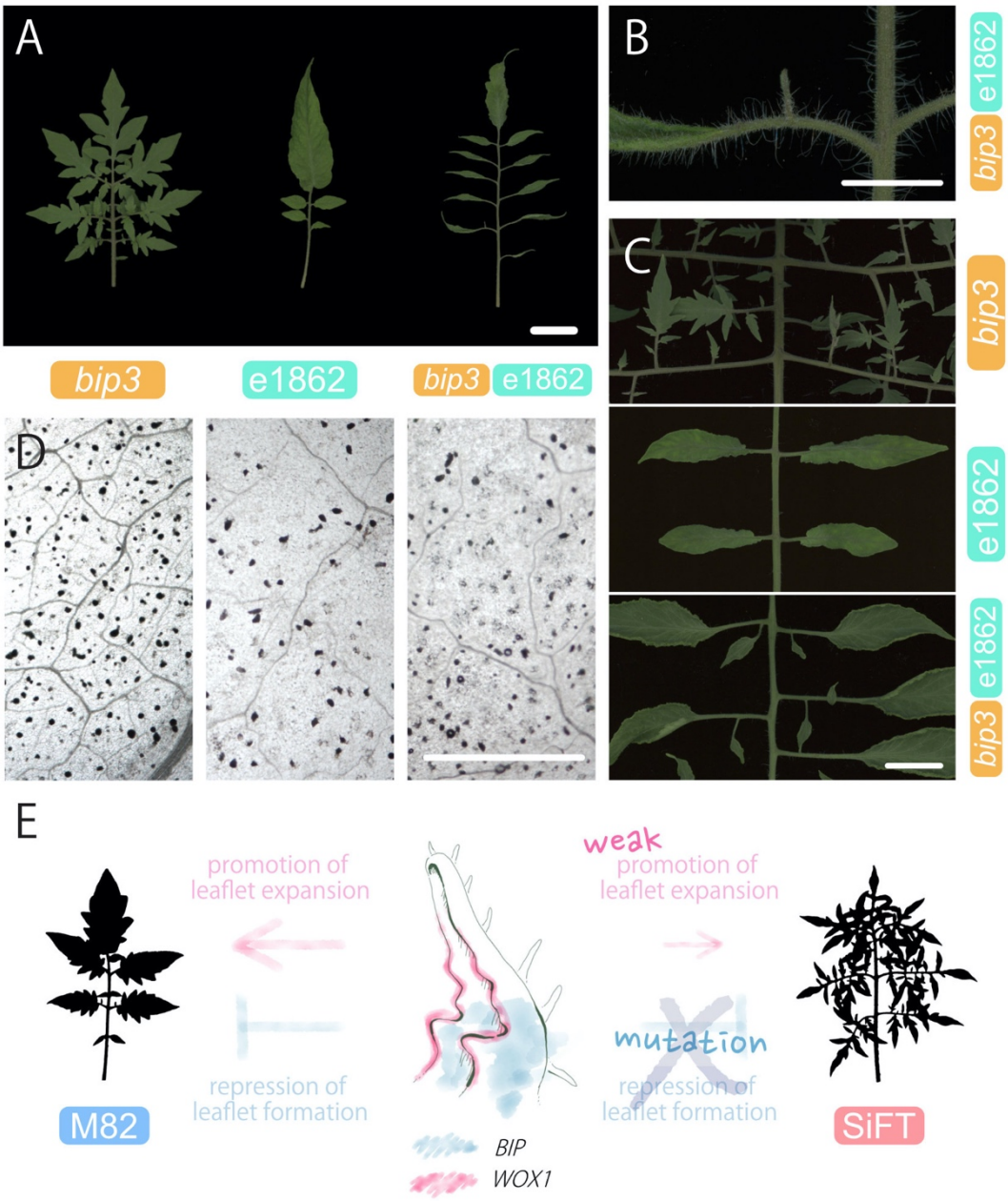

Figure 6. *bip sf* double mutant leaf phenotypes.

(A) Mature leaf morphology of *bip3* e1862 double mutant. From left to right: *bip3*, e1862, and *bip3* e1862 double mutant. The 4th leaves were used. (B) Close-up view of a secondary leaflet on a 4th leaf in the double mutant shown in (A). (C) Comparison of secondary leaflets on matured 6th leaf from 60 days old seedlings. (D) Cleared terminal leaflet images of *bip3*, e1862, and *bip3* e1862 double mutant. (E) A schematic model for leaf development in SiFT. Bars = 2 cm in (A) and (C), 1 cm in (B), and 1mm = in (D).

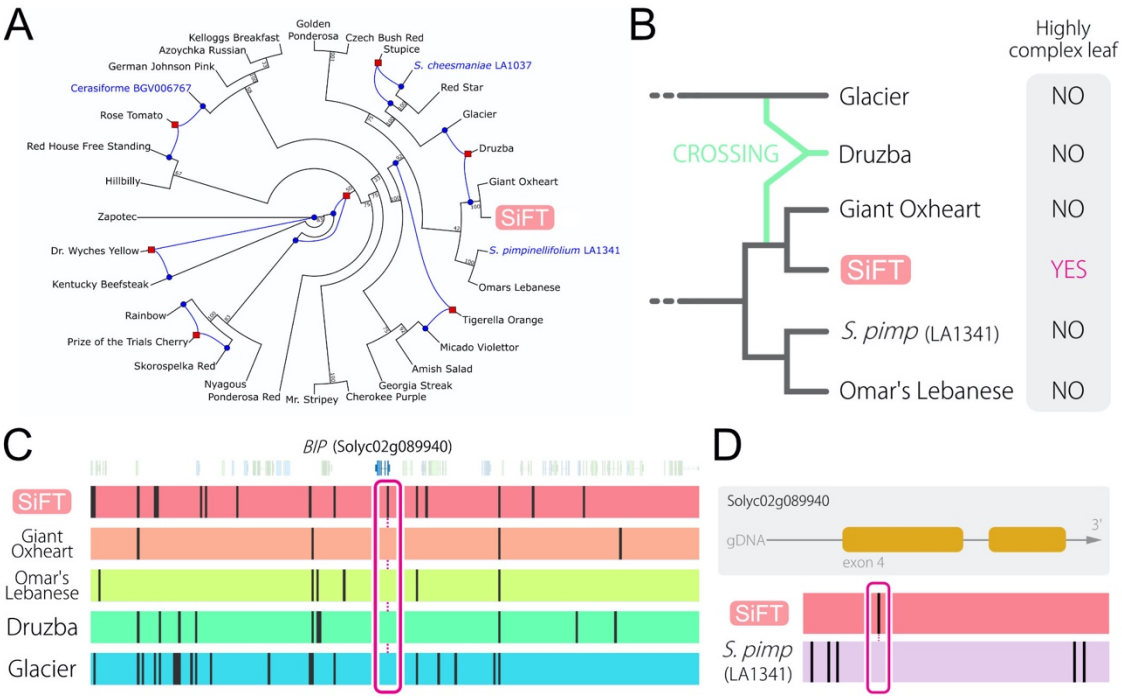

Figure 7. Reconstruction of breeding history and comparison of SNPs data.

(A) PhyloNetwork with sequences around the *BIP* locus on chromosome 2. The network describes various biological processes such as hybridization or introgression (Blue lines). The bootstrap values are indicated on branches (only those more than 50% are indicated on the tree). (B) Magnified view of the network shown in (A) focusing on SiFT. Comparison of SNPs data around *BIP* locus (Solyc02g089940) with heirloom tomatoes (C) and a wild species (D). Each vertical black line indicates a SNP.

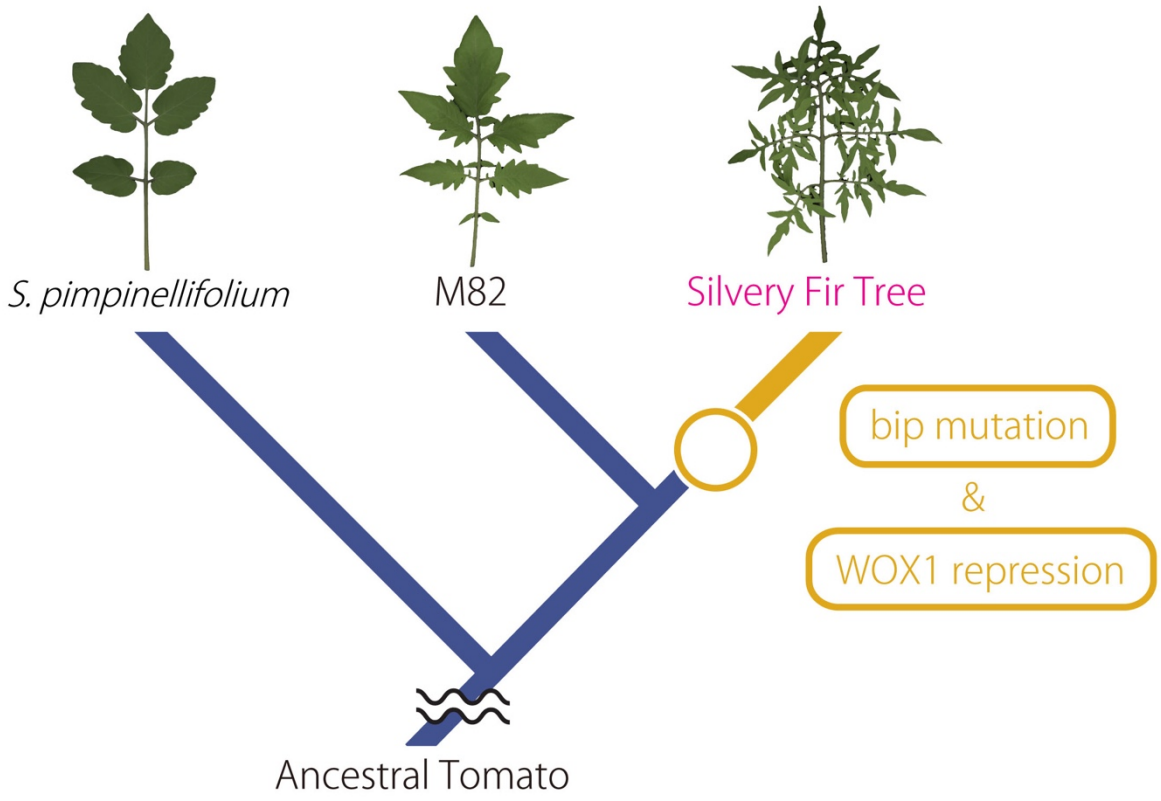

Figure 8. Breeding history and diversification of leaf shape in cultivated Tomato. Simplified phylogeny presented in Fig. 7 with leaf morphologies. Boxes indicate presumed key events during evolution. See text for details.